Check for updates

Original article



# Aircraft-level sensitivities of electric network component performance for (hybrid-) electric aircraft

Nicolas FM Wahler and Ali Elham

Proc IMechE Part G: J Aerospace Engineering 2025, Vol. 0(0) I–18 © IMechE 2025



Article reuse guidelines: sagepub.com/journals-permissions DOI: 10.1177/09544100251345167 journals.sagepub.com/home/pig



#### **Abstract**

Research on electric aviation energy networks tends to focus on either detailed studies of individual subsystems, or full-aircraft analyses that use highly simplified network (component) models. This paper aims to bridge that gap by performing sensitivity studies for various network parameters (HVDC cables, power converters, and motors), evaluating their effect on both the system and aircraft level. This is achieved through a combination of higher-fidelity explicit modeling of the network components and conceptual aircraft design software. This analysis is applied to a parallel-electric regional jet and a fully-electric commuter aircraft. The effects of parameter variations within literature-supported ranges are evaluated on component, network and aircraft mass for a given mission profile. Results show that the most influential parameters are the level of DC voltage in power transmission, the cable material, and the achievable mission-average efficiency of the electric motor. Individual component mass variations of over 100% can be observed within the investigated ranges; with variations of up to 10% of the aircraft mass for the parallel-electric jet. Aircraft mass variations for the fully-electric aircraft are up to 5%, with the required battery size due to component efficiency changes as driving factor. Results show that for large aircraft, the network is highly sensitive to power requirements. For small aircraft the network is more sensitive to mission energy requirements.

#### **Keywords**

Electric aircraft, energy network, electric propulsion, network components, sensitivity study, hybrid-electric aircraft

Date received: 10 May 2024; accepted: 29 April 2025

# Introduction

In recent years, the aviation world has experienced an ever growing interest in diversifying aircraft energy sources, and a move away from conventional fossil fuel propulsion. Electric aircraft are regarded as the most promising emerging technology for this. For General Aviation (GA), battery electric concepts have already led to promising results, some of which are fully certified and even in serial production. Larger aircraft, however, remain an area of active research, and the opportunities and challenges of electrification in this field are still being investigated. <sup>1–3</sup>

Preliminary design of (Hybrid-) Electric Aircraft (HEA) is often done through one of two approaches: either through low fidelity networks, which assume single efficiency values for whole networks, and specific energy and power densities<sup>4–6</sup>; or through higher fidelity models, which differentiate between components within their network architecture but still make use of simplified models with single efficiency values.<sup>7–10</sup> These simplifications in the modeling of network components make the integration easier, but fail to represent specific architectures and may misrepresent scaling opportunities.

A limited amount of studies exist that investigate the effects of changes in materials or performance of individual network components on the full aircraft-level size and masses. Studies investigating full-aircraft level influences and sensitivities are usually limited to high-level performance assumptions. <sup>11,12</sup>

Gesell et al.<sup>13</sup> have investigated the effects of hybridelectric propulsion systems on a regional aircraft concept for a variety of network architectures and power splits. Results show a breakdown of the resulting network component masses, with the battery, motor, and wiring being the most influential parameters on total aircraft mass. However, their network analysis simplifies power and energy density characteristics with assumed values for each component. A similar approach applied to larger

University of Southampton, Southampton, UK

#### Corresponding author:

Nicolas FM Wahler, Department of Aeronautics and Astronautics, University of Southampton, Southampton Boldrewood Innovation Campus, Building 176, Southampton SO16 7QF, UK.

Email: n.wahler@soton.ac.uk

aircraft with a turbo-electric concept is presented by Jansen et al. <sup>14</sup>. In this study, variations of component-specific power and density values show that motor/generator and wiring have the largest influences on network masses.

Kohler et al. 15 have performed detailed sizing of electrical machines and explored the design space for small propeller-driven HEA, with system voltage levels up to 600 V. Effects of other network components are mentioned, but not explicitly modeled. The influence of voltage variations on HEA is specifically investigated by Vratny et al., 16 modeling and investigating power electronics for an aircraft in steady cruise flight with a continuous cruise power of 6000 kW. This power level was chosen in line with estimations from the Voltair and Ce-Liner<sup>18</sup> concepts. Results identified an optimum propulsive system network voltage level between 3000 and 4000 V. Further research is advised to determine if these high voltage levels are feasible in aircraft design, as limiting conditions such as arcing were not investigated. A more detailed energy network was created by Ibrahim et al. 19 and applied to a turbo-electric aircraft to find an optimal operating voltage as function of motor speed to minimize total system mass. At low speeds, propulsion system mass was driven by larger mass requirements of the electrical machines and cooling system to create the required power, while for high motor speeds the size of the power electronics were dominant as required motor mass is reduced.

A variety of review papers discuss performance on a purely component level, and give outlooks for future materials and estimated performance improvements for network components. <sup>20–24</sup> Studies investigating more detailed network component performance within an energy network focus on individual aspects of these models, such as the choice of semiconductor materials and switching frequencies in the power converters. <sup>25–27</sup> Other studies have investigated the effect of higher voltage in the Direct Current (DC) cables and using Aluminum (Al) over Copper (Cu) as a conductor material for the cables. <sup>28,29</sup> However, these studies are only performed on a component or system level. The effects of these material choices on a full aircraft are not investigated in detail.

The objective of the presented study is to close the gap between these two types of research: full aircraft-level studies that use overly simplified network models, and investigations in performance variations limited to the component level. For this, a detailed energy network model with individual models for each major network component is used in combination with conceptual aircraft design software. The effects of network component design parameter variations on component, network, and aircraft masses are investigated in sweeps within literature-supported ranges for two case studies: A 50-passenger Boosted-Turbofan (BTF) regional jet and a 19-passenger Fully-Electric (FE) commuter aircraft.

## **Electric network components**

For this study, seven key design parameters are selected. The choice of these seven parameters is substantiated by both review papers as well as specific network studies that only focused on a single or low number of parameters from this list.

- Power converters
  - Semiconductor type/material
  - Semiconductor switching frequency
- Power distribution
  - Cable material
  - DC voltage
  - Cable length
- Electric motors
  - Overall efficiency
  - Maximum rotational speed

While the composition of the network will have a measurable impact on the final aircraft, the most important parameter to evaluate performance and credibility of a HEA design is the battery specification. As extensive literature regarding current and futuristic battery performance exists, the paper does not consider variations in this subsystem. Instead a performance value of 500Wh/kg is assumed for all aircraft designs. 31

Additionally, a number of papers investigate the effects of superconductivity for aircraft networks. 11,12,32–34 These papers provide a review of the current state-of-the-art regarding cryogenic propulsion systems, including aircraft design applications. Due to the high efficiency of superconducting wiring and machines, higher power transmission and power density for the machines can be achieved. This in turn increases the feasible design space and mission range for the investigated concepts. However, due to the low technology readiness level and plenitude of design challenges for the practical implementation of superconducting energy networks, this particular aspect of network type is not investigated in the paper.

## Power converters

In the power distribution systems of any electric network, power converters and regulators are necessary. Depending on the architecture, these converters can be of an AC/DC type (e.g. when using a power turbine to generate DC for distribution), DC/DC type (e.g. different voltage levels required by subsystems) or DC/AC (e.g. to power an electric motor). The performance of all power converters depend on their topology and semiconductor material.<sup>23</sup> Current high-performance power electronics technology is mostly based on Silicon (Si) semiconductor wafers.<sup>24</sup> The benefit of Si as material is low production cost, and hence its current ubiquitous use in power electronics. For ground based environments such as electric cars and other applications, Si-based appliances are thus a good fit.<sup>24</sup> In aviation, however, more stressors must be considered, due to the more hostile and fault-critical environment.

For these applications, Wide-Band Gap (WBG) semiconductors such as Silicon Carbide (SiC) are more appropriate. Benefits of SiC-based semiconductors include higher operating temperatures, lower leak current and

higher critical electric field strengths. 22,27 SiC-devices also exhibit a better radiation hardening, thus proving beneficial in high radiation environments such as high altitude flight and space environments.<sup>22</sup> A drawback of SiC-devices is the higher cost of the semiconductor material.<sup>24,27</sup> Furthermore, simply replacing Si-devices with a SiC equivalent is not fully exploiting the benefits that WBG devices can offer. For this, both the components and the system operating levels need to be adapted.<sup>24</sup> SiCdevices are able to operate at higher voltage levels and operating temperatures. <sup>22,24,27</sup> Thus, more power can be transformed by a smaller design, further increasing the suitability for aircraft applications. Higher breakdown voltages and allowable higher current densities allow a reduced wafer size and thus total system mass for SiCdevices. 11,20

Additionally, they can accommodate higher internal switching frequencies compared to Si-wafers. <sup>20,26</sup> The choice of switching frequency again can have a measurable effect on efficiency and system mass. Higher switching frequencies result in lower capacitance and inductance requirements for the component, but will result in higher switching losses and thus a lower efficiency. <sup>26</sup>

#### Power distribution

Current commercial aircraft commonly have two different electric networks: 115 V Alternating Current (AC) and 28 V Direct Current (DC) to power their internal systems. The Modern aircraft such as the Boeing 787 operate on voltages up to 540 V AC<sup>27</sup>. Traditional systems are limited in voltage by the arcing voltage in accordance with Paschen's law. A system voltage of less than 327 V will never produce an arc when using air as insulator, and is thus a sensible limit for safety critical applications.

However, for a credible electric propulsion system, these voltage levels are insufficient. Higher power requirements necessitate higher current flows. Increase in current leads to higher temperature and transmission losses, as well as requiring larger cables and insulation. Hence, in aviation, it is of utmost importance to reduce the current flow in the wiring.

With modern insulation, higher system voltages of up to 3 kV are realistic. 16,22 Studies using cryogenic technology investigated voltages of up to 10 kV, however these technologies are still at a low Technology Readiness Level (TRL). Furthermore, a simplification of the aircraft electrical system from a combination of AC and DC grids to pure higher voltage DC grids can have other synergistic effects. For aircraft systems, DC is more relevant. Avionics currently accept an AC voltage, but that is internally converted to a DC voltage. A DC grid furthermore has a higher system stability and power quality, 34 and requires only two cables instead of three for an AC system 28 for a reduced mass.

Currently, copper is the most widely used material for conductors. Besides its low cost, copper furthermore has a good current density and conductivity.<sup>34</sup> An emerging alternative material is aluminum. Aluminum has a lower

current density, and thus requires larger cables. Due to its lower density, the total cable mass is still reduced. 16,28 A drawback is that aluminum cables have a higher power transfer when arcing occurs, compared to copper. 28 Current Federal Aviation Authority (FAA) regulations limit the use of aluminum cables in certain areas, such as fuel systems and engines. 28 Aluminum cables are seen preferable for high-power applications and fully-electric aircraft, and already found some use in current transport aircraft designs. 16

## Electric motors

A wide selection of electric motor types exist to cater to a plethora of different applications. For aviation use as propulsors, asynchronous, switched reluctance or polyphase synchronous machines are good options. 11 Of these options, the polyphase synchronous machine is the most suitable, as it has a high energy and mass efficiency. The most common variant is the polyphase permanent magnetic synchronous machine (PPSM), which is already commonly used in electric aircraft designs<sup>35</sup> and included in the network model. The main goal of electric machine design for aircraft applications is to create the highest power densities and efficiencies. On a machine level, this translates to fitting the flux required to deliver the demanded power into the smallest possible casing. This can be improved by reducing the air gap between rotor and stator of the machine. 19 Further improvements can be made to the rotor component by for example utilizing permanent magnets instead of windings.<sup>11</sup>

For a given power setting, the torque that the motor can provide is depending on the rotational velocity (RPM) of the rotor. Changes in design RPM have an effect on the motor mass. Increasing the rotor RPM leads to lower rotor masses and higher efficiencies. However, the higher current and centrifugal forces can lead to an increase in total mass due to material limitations. <sup>19</sup> In general, total motor mass varies inversely with the rotor speed. <sup>19</sup>

Overall motor efficiency is a major parameter for electric aircraft design and performance studies. Most current conceptual studies are assuming rubber motors with constant power-to-weight ratios. This is a valid approach when the motor is always designed for the same rotational speed. If this speed is changed, more detailed models to simulate varying power requirements throughout the full mission are necessary. As electric machines have a lower efficiency if they are operated below the design point, the average efficiency throughout a full flight mission will also be lower than the nominal efficiency and thus should be accounted for in a credible aircraft design concept.

# **Methodology**

The sensitivity study presented in this research is based on detailed simulation models of the propulsive and electric network. A high-fidelity energy network model was created for the simulations, capable of simulating all individual components in a detailed manner.<sup>30</sup> This is opposite to energy network models commonly used in conceptual design such as the one implemented in SUAVE,<sup>7</sup> which are simplistic and trade a reduction in model fidelity for a low evaluation time. This section provides a short summary and overview of the relevant network modules.

A more detailed description of the full model capabilities, its individual component models, and verification data is provided in <sup>30</sup>. Due to this higher fidelity level, the network model is not fully modular unlike models commonly used in conceptual design software, but is combined into pre-fabricated basic network architectures that are used in the case studies. The particular fully-electric and parallel-electric architectures used in this study are shown in shown in Figure 1.

The fully-electric architecture consists of electric motors driving conventional propellers of the aircraft. The mission energy is stored in and provided by battery packs located in the wings. Due to the high battery mass, this network is most suitable to small GA or commuter aircraft.<sup>36</sup>

The parallel-electric architecture is a variant combining primary propulsion through a gas turbine engine and power from electric motors. The implementation in this model is that of a boosted-turbofan. The main energy is provided by a twin-spool turbine engine, with an electric motor as a performance booster attached to the lowpressure turbine to provide additional power. As this engine uses a turbofan for the propulsive power, it is suitable for higher flight speeds and cruise altitudes compared to the previous architecture. It can also be more easily scaled up to higher power requirements making it more suitable for larger aircraft. The electric motor is connected to the low-pressure spool. This architecture allows the electric motor to be used as an accelerator/ booster to support the turbofan in partial load and transient maneuvers.

## **Propulsors**

*Propeller.* The propeller design and its respective performance computations are performed using a modified blade element momentum theory (BEMT) model.<sup>37</sup> Amongst the implemented modifications to the classic BEMT-models are a detailed modeling of the tip loss factors<sup>38</sup>

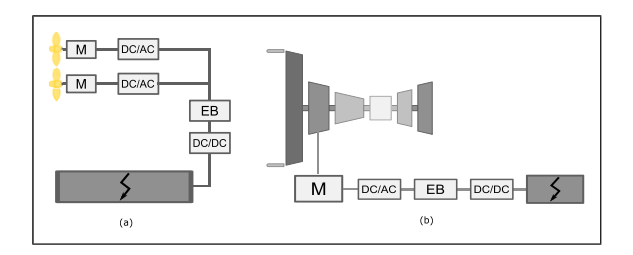


**Figure 1.** (a) Fully-electric architecture (b) Parallel-electric architecture . M: Motor, DCDC/DCAC: Converter, EB: Electric Bus.<sup>30</sup>

as well as improved 3D-effect models.<sup>39</sup> With this tool, it is possible to analyze the propeller performance for all stages of the simulated flight profile, both in the design point and in off-design conditions.

Gas turbines. The gas turbine analysis is based on a cycle-computation tool. <sup>40</sup> In the calculation process each engine component is treated as a separate unit and is linked to the other units by input and output parameters to form the overall engine system. Therefore, the components will be calculated sequentially. The tool makes use of integrated gas tables and functions for other material values.

The general performance simulation process, which is representative of the calculations for a pure gas turbine is modified to accept hybrid architectures. For the electrically-boosted turbine, the energy balance equations of the turbine stages are modified such that the power of the connected electric motor is considered.

The basic cycle tool computes the on-design performance of the engine. For the consideration of offdesign operating points, an interpolation algorithm is implemented.

## Electric machines

The electric machine converts electrical energy into mechanical energy and thus represents the interface between the power electronics and the mechanical drive unit. There are many different possible machine topologies and some of them differ greatly from one another. One goal in modeling the electric network is to make the model for the electric machine as modular as possible, so that it is possible to exchange the electric machine in the model and investigate the effects on the electric drive and the entire aircraft. As an adequate measure to compare different machines and their performance, machine rotary thrust is used as prime design parameter.

All machines are implemented in parametric form to allow easy scaling of the components to fit the respective needs of the investigated aircraft. In the design point, the machine is defined by the required power of the propulsive system, and constrained by its maximum rotational speed. The torque of the electric machine is then determined by a constant rotary thrust, which determines the electromagnetic load of the machine, and a certain geometry. The installation space, which determines the geometry of the machine, is specified by a diameter and an axial machine length.

To determine the efficiency  $\eta$  of the machine and the total power that must be supplied to the machine, the internal losses are calculated and scaled. Scaling of the machine is done in both axial and radial directions, using the scaling factors  $k_{ax}$  and  $k_{rad}$ . The copper losses in the slot and the iron losses are considered. The copper losses are calculated from the current I and the resistance  $R_s$  as shown in equation (1). The copper losses  $P'_{Cu}$  are proportional to the resistance  $R_s$  which changes proportionally to the axial length of the machine. It follows that the copper losses  $P'_{Cu}$  are also proportional to the axial machine length.

With radial scaling, the copper losses  $P_{Cu}$  remain constant. The electrical resistance  $R_s$  is inversely proportional to the cross-sectional area which changes quadratically with radial scaling. Since the current I changes proportionally with the radial scaling, but the copper losses  $P_{Cu}$  depend quadratically on the current, these effects cancel each other out.

$$P'_{Cu} = k_{ax} P_{Cu}$$

$$P'_{Cu} = R'_{s} I'^{2} = \frac{1}{k_{rad}^{2}} R_{s} k_{rad}^{2} I^{2} = P_{Cu}$$
(1)

The iron losses depend on the soft magnetic material, the flux density distribution and the frequency. If the material is assumed to be geometry-independent and the flux density distribution and frequency are kept constant, the power losses  $P_{Fe}$  remain constant and the iron loss power can be scaled over the volume. Since the volume changes proportionally with axial scaling and quadratically with radial scaling, the iron losses  $P_{Fe}$  are scaled according to equation (2).

$$P'_{Fe} = k_{ax} P_{Fe} P'_{Fe} = k_{rad}^2 P_{Fe}$$
 (2)

The total motor efficiency is then found as the fraction of usable power to total required input power given by equation (3).

$$\eta = \frac{P_{output}}{P_{Cu} + P_{Fe} + P_{output}} \tag{3}$$

In order to find the optimal radial and axial size for the electric machines yielding the highest efficiency, an internal optimization routine is used. The maximum allowed rotational velocity of the machine as well as axial and radial size limits are used to constrain the geometry. The maximum attainable motor efficiency is thus a function of the required power and varies depending on the specific application.

### Power electronics

The increasing number of electrical loads on board of aircraft naturally lead to a greater number of power electronics converters. Therefore, power converters design with an emphasis on weight and volume minimization besides the efficiency optimization is crucial. While some work on high power density converters has been reported in the literature, most of this work focuses on minimizing volume, <sup>26,41</sup> but not on weight reduction. The description of the latter is therefore a main feature of the methods presented here. The basic types of power electronics converters considered within this model are:

- Inverters (DC/AC-converters), which change the direct current from the High-Voltage Direct Current (HVDC) board net to alternating current needed for the electric machines
- Rectifiers (AC/DC-converters), which are needed to interface between an electric generator and the rest of the energy network, and

 DC/DC converters, which are needed to interface between different voltage levels, for example for connecting a battery system to the other parts of the energy network.

The modeling of these power converters aims to estimate the resulting total losses of the converters and the resulting weight and volume. This performance estimation can be done at different levels of detail and using different methods. The major sub-components that are found in all converter types are identified and analysed for weight, volume and losses, while acconting for non-linearities like different circuit topologies and semiconductor materials. <sup>26,42,43</sup>

Power semiconductors. An important aspect in the modeling of converters is the selection of the power semiconductors, which directly influence the losses of the converter system. 42 Different semiconductor technologies are investigated: conventional Si Insulated-Gate Bipolar Transistors (IGBTs) and SiC WBG Metal-Oxide-Semiconductor Field-Effect Transistors (MOSFETs). In order to describe the properties of these different semiconductor materials, a database of characteristic semiconductor half-bridge modules, made of different materials by different manufacturers, is created. Once the electrical characteristics like modulation index, switching frequency and current, voltage peak and root mean square values have been determined for each converter topology to be considered, the power losses are calculated analytically. 41,43,44

Inductors. For the inverter it is assumed that the line filter, consisting of a single inductor on each phase, is the output filter's determining component in weight and volume. 45,46 Especially in higher power power converters, the size and thus mass of this filter cannot be ignored. 47 The line inductance is calculated analytically as a function of the desired current ripple, 48 voltage and switching frequency. 48 The inductor's shape and size is determined through a sizing algorithm. 49 This algorithm is used to determine the geometric dimensions as well as core and conduction losses using a thermal equivalent circuit. The total losses in the inductor are calculated. Considering the different densities of the used materials in core and windings, the mass is derived.

Capacitors. Depending on the number of levels of the converter, the DC-link capacitance for the inverter<sup>26</sup> and the maximum required capacity for the interleaved synchronous converter<sup>50</sup> are calculated analytically.

During the selection process, each capacitor in a component database is assessed by determining the number of single capacitors that would be needed to be paralleled to meet the required capacitance value. The capacitor arrangement with the lowest resulting losses and mass is selected. 45,49

Cooling system. Since a large part of the losses in the converter is expected to be generated by the power

semiconductors, this is considered the sizing condition of the heat sink. Heat sinks and dissipation are not explicitly investigated in this study, hence a single heat sink is assumed for all switches. The thermal equivalent circuit contains only the loss generating switches with a given junction-sink and junction-case thermal resistance plus a thermal resistance of the thermal interface material in between the case and sink. Given an ambient operating temperature and maximum allowed junction temperature for the semiconductors, the needed thermal resistance for the heat sink can be determined. For the volumetric modeling of the heat sinks the Cooling System Performance Index as a figure of merit is used. 43,49 A specific heat sink fill factor can then be used to approximate the heat sink weight from the heat sink volume.

#### Power distribution

The design of the HVDC electric power system is based on normative specifications for the current-carrying capacity of insulated conductors. The model is sensitive to conductor material, voltage level and wire length. Using a thermal equivalent circuit and the required electrical and material input parameters, a cable consisting of a homogeneous insulation material and a conductor is designed. For a defined maximum permissible conductor temperature, the conductor cross-section is sized for minimum total mass.

# Energy storage

A detailed battery model sizing the full stack with cells in series (power or energy requirements) and parallel (voltage requirements) is included in the model. In order not to influence (or overshadow) the resulting network component sensitivities, for this study a fixed performance value of 500*Wh/kg* is assumed for all aircraft designs.<sup>31</sup>

The weight of the peripheral systems (e.g. cooling system and electronic components such as connectors, etc.) is considered and a weight ratio of 1.43 is used to convert the cell mass to the system mass.<sup>52</sup> Similarly, a ratio of 1.3 is used to convert cell volume to system volume.

#### Aircraft evaluation

The core performance simulation of the aircraft is performed within the SUAVE software. SUAVE is a mission simulation tool created by Stanford University. The aircraft is modeled through basic geometric parameters as well as a model of the propulsion system. The design mission is divided into multiple individual segments with individual configuration and performance options. Each segment is further discretized and an iterative solver is used to determine the required thrust and angle of attack to achieve a trim condition for each discretization point. The found thrust and aerodynamic conditions are used to investigate the behavior of the aircraft throughout the full mission. SUAVE also includes a mass breakdown module that estimates the masses of all major aircraft components.

SUAVE as a mission analysis tool will always simulate the mission over the full design range, as well as require as much power from the energy model as the internal iterator requires to converge at a specified flight phase. This can result in negative charges of the batteries in case the mission is longer than the on-board batteries allow, or power requirements that can exceed the maximum power available. Hence, additional consistency constraints are introduced to ascertain that the final design will be physically possible. The internal iteration loop simulates the given mission and computes the aircraft performance including energy requirements for the full mission. It then applies a mass breakdown of the aircraft components to check if the aircraft is consistent mass-wise for the flown mission. If not, then the energy network is resized based on the required mission energy for the battery mass, and the initial design point power loading for the engines. To account for changes in the Maximum Take-Off Mass (MTOM) of the aircraft, the wing is also resized in accordance with the initial design wing loading. Resizing wing and engine with the original design point's specified wing and power loading assures that the overall aircraft design point does not change within the iterations.

This iterator is used on a range of cases with varying input parameters for electric network components of a common baseline aircraft design. The goal is to compare the resulting network component masses and aircraft MTOM changes due to these variations in network parameters.

Within the network component models, some individual sub-components are chosen based on the network inputs, for example depending on voltage and semiconductor material, different actual semiconductor types can be selected. As such, the performance of specific physical components within the model can change depending on external inputs. This can then lead to small differences in the internal efficiency or mass of a system, affecting the battery and hence aircraft mass. While this is a desired behavior of the higher-fidelity network model, it can result in slightly non-monotonous behavior in the sweep graphs.

#### Verification

The network and its individual components are verified against current literature. The full network-specific results are published in <sup>30</sup>, and only key points are repeated here.

All individual network components are unit tested against commercial products or literature results. The full aircraft model and sizing procedure is verified against a full aircraft mission simulation of the same design using a different analysis software.

Figure 2 shows a comparison of the propeller module results for power  $(C_P)$  and thrust coefficient  $(C_T)$  against advance ratio. The results are compared to literature values by Adkins and Liebeck<sup>38</sup> and the tool Javaprop<sup>2</sup>. Results show a good agreement with the literature results for this propeller design. For very low advance ratios, differences are expected with Javaprop as the program includes corrections to the pulse equation that are currently not considered in this model. Figure 3 shows a comparison of the gas turbine model with the commercial software Gasturb<sup>3</sup>. For total temperatures in the range of up to  $1000 \,\mathrm{K}$ , maximum differences of about  $3 \,\mathrm{K}$ 

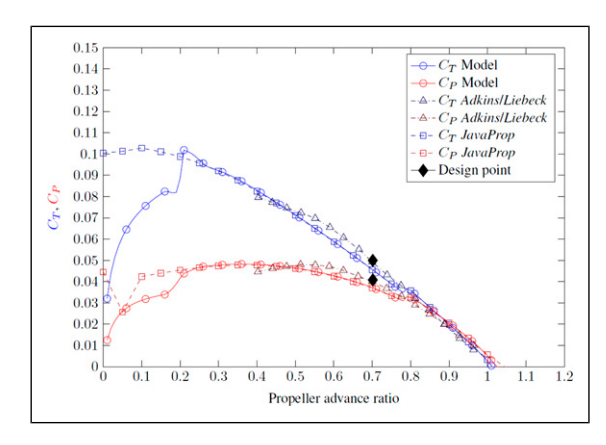


**Figure 2.** Propeller analysis against advance ratio comparison for model, literature and JavaProp for power and thrust coefficients.<sup>30</sup>

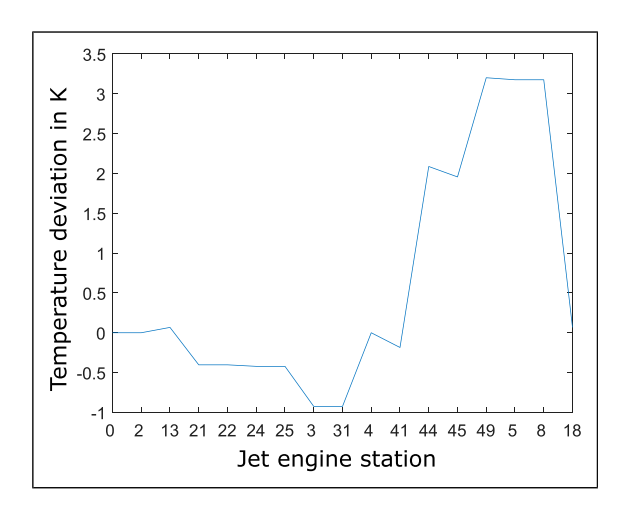


Figure 3. Temperature differences between Gasturb and the model results along the turbine.<sup>30</sup>

can be observed in this comparison, hence showing the accuracy of the implemented gas turbine model.

The electric machine model is verified against a high-temperature superconducting (HTS) machine from.<sup>53</sup> The reference machine is designed to provide a power of 3031 kW to drive a fan which imposes limits on the maximum size of the machine. The comparison of size and key parameters between the reference machine and the model results are shown in Table 1. The model results show good overall agreement with the reference, with small deviations in the rotational velocity (+3.3%) and line current (+4.2%).

Table 2 shows results for the power converter models. The DC/DC converter is modeled as interleaved bidirectional step-up converter for automotive applications and utilizes three half-bridges reaching a power density of 25 kW/kg at 100 kW rated power and 100 kHz switching frequency. The DC/AC converter represents an air-cooled 40 kW SiC-inverter using the conventional 2-level topology at a 100 kHz switching frequency. Both results show good agreement with the literature values. Small discrepancies are expected due to the differences in specific modeling approach and assumptions made for the replication.

 $\begin{tabular}{ll} \textbf{Table I.} Verification results using a representative HTS \\ machine. \end{tabular}$ 

Property	Reference machine <sup>53</sup>	Calculation
Power	3031 kW	3031 kW
Speed	4400 rpm	4547 rpm
Diameter	350 mm	350 mm
Axial length	269.23 mm	270 mm
Line current	2000 A/cm	2083 A/cm

**Table 2.** Model verification of power converters.<sup>30</sup>

Parameter	DC/DC	DC/AC
Design power	100 kW	40 kW
Design switching frequency	100 kHz	100 kHz
Literature power density	23 kW/kg	10 kW/kg
Model power density	25 kW/kg	9.5 kW/kg

#### Results

The energy network model is applied to two aircraft case studies - a BTF 50-seater regional jet and a FE 19-seater commuter aircraft - to evaluate the effects of changing network parameters. The baseline aircraft were designed using the Initiator aircraft design software. For both aircraft, the defined baseline network setup is selected using current components and material choices applicable for such a network. All variations are set relative to this baseline case to showcase the effects of changing assumptions, or using components which are not currently commonly used in electric aircraft networks.

## Boosted turbofan regional jet

The first case study considers a regional jet. The aircraft is designed with 50 seats and a twin BTF layout, shown in Figure 4. Table 3 gives some key performance parameters characterizing the baseline aircraft.

Table 4 shows the selected input parameter choices taken to simulate the electrical components of the propulsion architecture for this baseline case. The switching frequencies of the power converters and the semiconductor materials for the DC/DC and AC/DC power electronics power converters have to be chosen in combination to yield a consistent set. The chosen frequencies are on the lower side of relevant values. This allows an evaluation of an increase in frequency as well as a change in materials, while still being in a feasible range for both parameters. The 2LC inverter topology is a good representation for the required performance. Regarding the wiring, it is assumed that the batteries are placed within the wing and center fuselage, in accordance with the baseline design in Figure 4. Thus, the total required HVDC wiring length can be kept low. Cu is currently the most common material for cable applications due to its high conductivity and ductility.

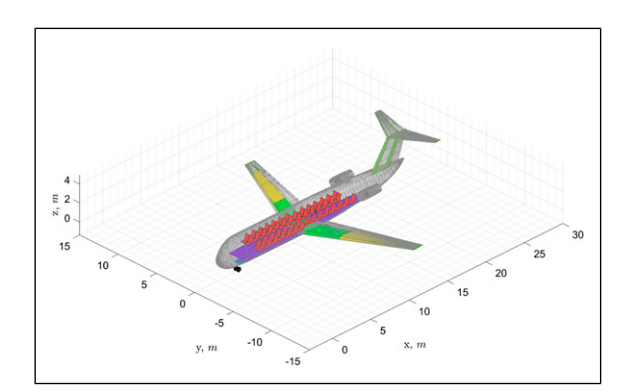


Figure 4. 50-passenger BTF regional jet baseline design.

Table 3. Key design parameters of the BTF regional jet.

Parameter	Value
Wing loading	4682.3 N/m <sup>2</sup>
Thrust-to-weight ratio	0.193
Electric motor power loading	0.0677 N/W
Number of passengers	50
Cruise speed	207.6 m/s
Cruise altitude	10668 m
Wing aspect ratio	8.43
Wing taper ratio	0.32
Wing sweep	22.5°

For this BTF concept, the electric motor is only used to support the gas turbine engine as primary propulsor. Throughout the mission, the motor is used at 76%-95% of its design power throughout the climb phases and at 34.5% in cruise. This corresponds to 18-30% of total propulsive power in climb and 16% in cruise. The electric booster is not used in the descent phases. The water cooled PPSM is selected as a realistic option for a currently available machine. It provides a good tradeoff between required size (and thus mass) and delivered power. PPSMs are commonly used for applications with the given power requirements. As the actual dimensions of the machine are defined by two input parameters in order to allow a fitting to available space within the given aircraft design, the machine was sized to be attached to the engine as shown in Figure 4. The provided design is intended for a service entry between 2035 and 2050. It includes assumptions for an increase in battery energy density,31,58 in order to provide a realistic concept for a futuristic, more sustainable aircraft.

The resulting aircraft is presented in a mass breakdown in Table 5, including a detailed breakdown of the individual network components and their contribution to the total masses. The Operational Empty Mass (OEM) includes the energy network with the installed batteries. The table is provided to allow for a better judgment of the relative influence of parameter variations on the final aircraft. Even systems that might seem small based on this table may have a sizable impact on

**Table 4.** Electric network sizing input data of the BTF regional jet.

Parameter	Value
DC/DC & AC/DC converter switching frequency	30 kHz
DC/DC & AC/DC semiconductor type	Si
Inverter topology	2LC
DC voltage level in HVDC subsystem	2000 V
Conductor material	Cu
Length of HVDC wiring	10 m
Number of batteries	2
Electric machine topology	PPSM
Cell level energy density of battery system	500 Wh/kg
Rated total power of electric machines	5.59 MW
Total required trip energy	11.8 GJ

Table 5. Mass breakdown of the BTF regional jet baseline.

	Mass [kg]	%MTOM	%Network
МТОМ	35,385	100.0	_
OEM	28,282	79.9	_
Fuel	1803	5.10	_
Network	14,635	41.4	100.0
Battery	8790	24.8	60.1
Motor	1622	4.58	11.1
HVDC	1122	3.17	7.67
DC/DC	216	0.61	1.48
DC/AC	393	1.11	2.69
Turbine	2491	7.03	17.0

the final results, due to changes in size and efficiency, which in turn affect other network components in a snowball effect.

Power converters. The first sensitivity study concerns the semiconductor materials and switching frequencies of the power electronics components. The results for Sibased systems are shown in Figure 5, SiC-based systems are shown in Figure 6. The legend on the left side of all following plots is used for all masses except for the specifically analyzed system. The legend on the right side of the plots is only applicable to the specifically investigated system.

For both curves, a general decrease in DC/AC and DC/DC converter mass for increasing switching frequency can be observed. The higher the switching frequencies, the more power can be transmitted for a given size, and hence the total system can be smaller and lighter.

However, higher switching frequencies also reduce the efficiency of the power conversion. Thus, while the converter mass is reducing for increasing frequencies in Figure 5, it can be seen that beyond about 60 kHz, the total network mass is increasing again. This shows the optimal operating range for Si-based power converters to be

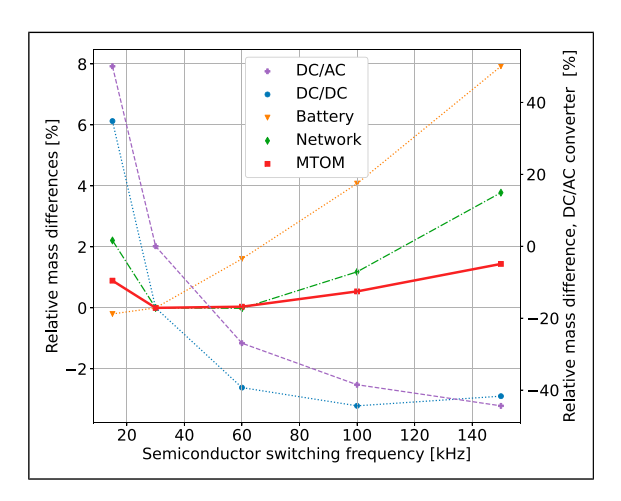


**Figure 5.** Effects of switching frequency variations using Sibased power electronics.

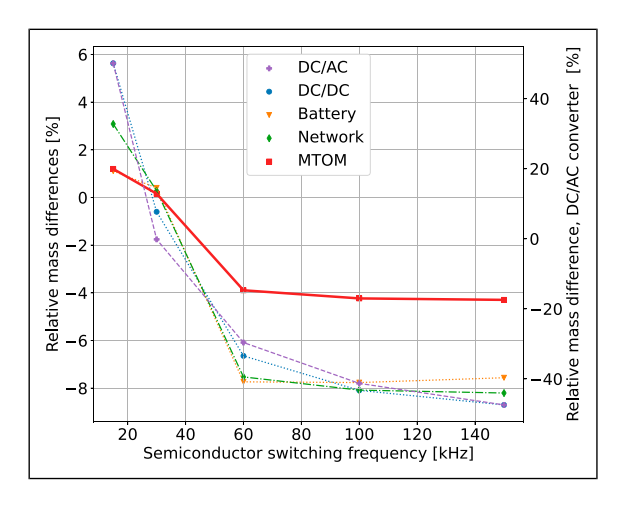


**Figure 6.** Effects of switching frequency variations using SiC-based power electronics.

between 30 and 60 kHz. The power converters are only a small part of the whole system and hence changes in mass, while in the order of +6% to -3% for the DC/DC converter and +55% to -45% for the DC/AC converter over the whole range of investigated frequencies, have only a minor result on the actual MTOM of the full aircraft. Due to the reduction in conversion efficiency at higher frequencies, more energy needs to be stored in the battery cells and increase their mass. This has an increasingly dominating effect counteracting the decrease in converter mass, leading to an overall increase in MTOM.

For the SiC-based results shown in Figure 6 the general trend of a reduction in converter mass for higher switching frequencies can be seen as well. For the same switching frequency as the baseline case, the differences in converter mass are in the order of 5% compared to Si-based systems, with a similar MTOM. However, these WBG devices are capable of handling much higher switching frequencies at smaller losses in efficiency. Hence, while the same efficiency-mass trade-off can be observed as with the Si-based results, the effects

of both are much smaller and cancel each other out, leading to a nearly constant total network mass, and thus MTOM. Another interesting note is that the SiC results show a higher total mass for low switching frequencies of 30 kHz and below. Compared to the baseline case, the MTOM is 1% higher using SiC with an increasing difference as the frequency is lowered, showing that SiC semiconductors preferably operate at least at 30-40 kHz or higher. Utilizing WBG semiconductors at high switching frequencies can decrease the MTOM for this BTF design by approximately 4%.

Power distribution. Figures 7 and 8 show the effects of increasing the HVDC voltage for Cu and Al cables, respectively. Figure 7 shows a monotonously decreasing trend of all parameters as the voltage increases. Higher voltage results in lower currents flowing through the wiring, and hence the cable is smaller and lighter. While this also increases the potential for arcing between wires and thus requires more insulation, the net effect is still positive. An asymptotic behavior can be seen as well. Increasing the voltage beyond 1500 V will deliver diminishing improvements in the cable masses, but requires larger and heavier insulation. The necessity of increasing voltage from the current HVDC systems using 540 V is also evident, despite this voltage level not being explicitly shown in this graph. Increasing the voltage from 1500 V to 3000 V decreases the HVDC wiring mass from +75% to -55% of the baseline value. Although an integral part of the electric network, the HVDC wiring mass is not relevant compared to the battery masses. Over the investigated range, the battery mass decreases by approximately 15%, showcasing the large improvements in transmission efficiency that can be achieved with higher voltages. The combination of a lower cable mass and visibly improved transmission efficiency results in overall MTOM variations of about 10%, proving that this is a highly influential parameter for any successful aircraft concept.

Figure 8 shows the same voltage range using Al as conductor material. Observing the scale on this plot immediately shows the inherent benefit of using Al cables. At the baseline voltage, the Al cables result in 70% lower mass than the Cu equivalent, 11% lighter batteries and a 7% reduction in MTOM. Similar trends as for the Cu wires can be identified as the voltage varies. While the advantages over Cu are evident for each voltage level, the Al cables show smaller sensitivity to voltage changes. Over the full range, the Al cable mass decreases by 40%, which - while still a large reduction - is much less than the relative change for the Cu cables. Al has a lower current density than Cu and thus needs a thicker cable to provide the same total power. It also has a lower density, which counteracts the increase in cable volume and still nets a large positive effect. These two effects result in a shallower slope for the Al cable mass changes. The MTOM changes are small for voltages higher than 2000 V, indicating that on

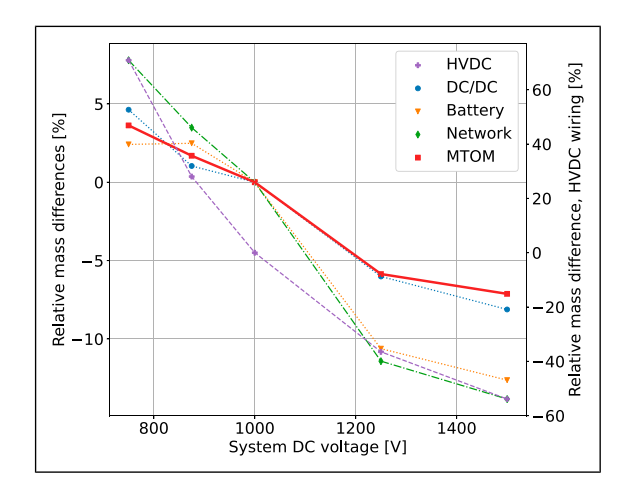


Figure 7. Effects of DC voltage variations using Cu wiring.

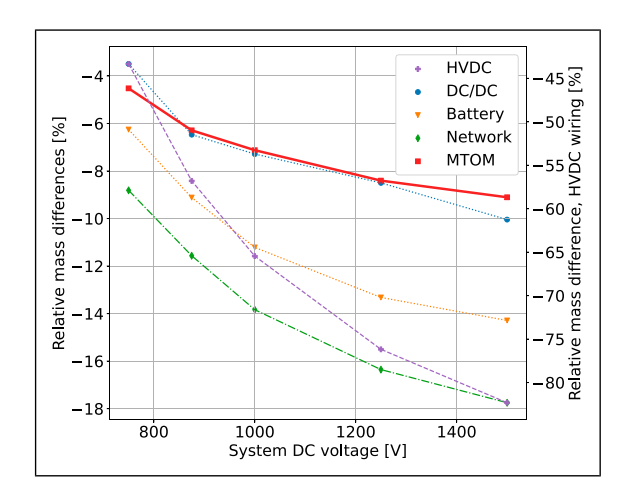
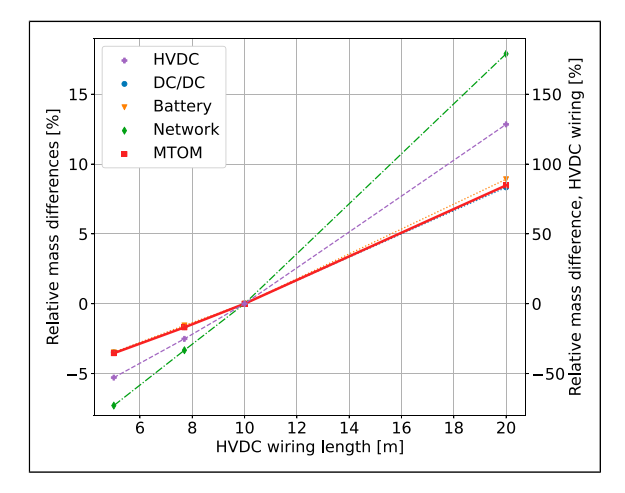


Figure 8. Effects of DC voltage variations using Al wiring.

a system level high voltages for Al cables are less relevant.

Both figures highlight the relevance of having an HVDC system with a voltage as high as feasible, and to consider Al wiring in future aircraft concepts. The potential improvements of up to 8% MTOM for this BTF can have a major influence on the final feasibility of an aircraft concept.

Figure 9 shows the effects of Cu cable length on the network. In the baseline design, the batteries are placed in the wings, close to the engine connection points. Thus, a total HVDC wiring length of 5 m per engine was assumed. However, depending on the design, batteries can also be placed in pods under the wings or in the fuselage, quickly increasing the required HVDC cable length. The results show a direct and linear correlation between the cable length and mass. Doubling the cable length increases the cable mass by 125%, while MTOM increases by about 8%. The results for MTOM and the battery are nearly identical, indicating a strong correlation between them. An increase in length also has an influence on the transmission efficiency, and hence it can be seen that the battery mass has a slightly larger slope than the



**Figure 9.** Effects of HVDC cable length variations using Cu wiring.

other parameters, albeit not a very pronounced difference at these cable lengths yet. Further increases would lead to a larger difference. On the other hand, decreasing the required cable length to half the nominal value leads to a 55% decrease in cable mass and a 4% decrease in MTOM.

The results in Figures 7, 8 and 9 show that the energy distribution has a visible effect on the final aircraft size. The location of the batteries needs to be considered carefully in order to reduce the required HVDC wiring length as this can have a visible effect on the final aircraft mass and hence power requirements. These penalties can be remedied by designing for a high voltage system and opting for Al cables. However, current safety and certification requirements (e.g. by the FAA) are limiting both of these design parameters and their application need to be considered carefully for a credible aircraft design.

Electric motor. As a major component of mass and size in electrified aviation, improving and increasing motor performance is a highly active field of current research. In conceptual design, electric motors are commonly characterized by a fixed gravimetric power density and a fixed efficiency figure. More advanced simulations may include simple motor models that are able to size the motor based on its actual geometry and simulate the changing motor efficiency at different power levels throughout the full mission profile.

Figure 10 shows changes in the masses due to different fixed motor efficiencies. These results showcase how simple models would simulate and assess the effects of motor performance on the full design. Clear trends show that for a higher efficiency, the masses of all components and the MTOM have a monotonous decreasing trend. The inverted triangle shows the MTOM result using a more sophisticated motor model. The motor is based on a PPSM machine and sized within the iteration loop to deliver the required nominal power at its design point. An optimization routine within the

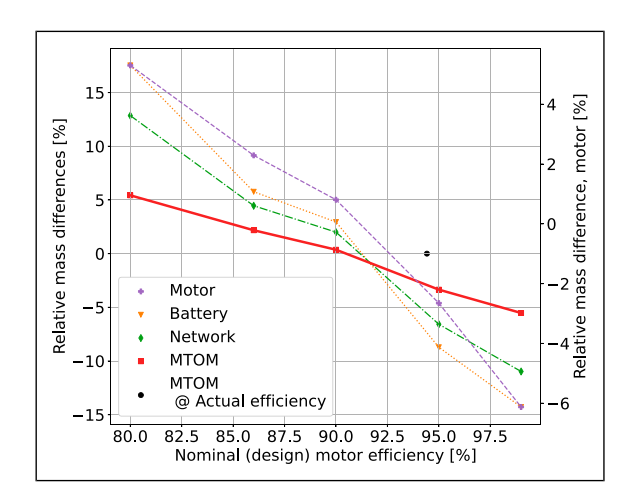
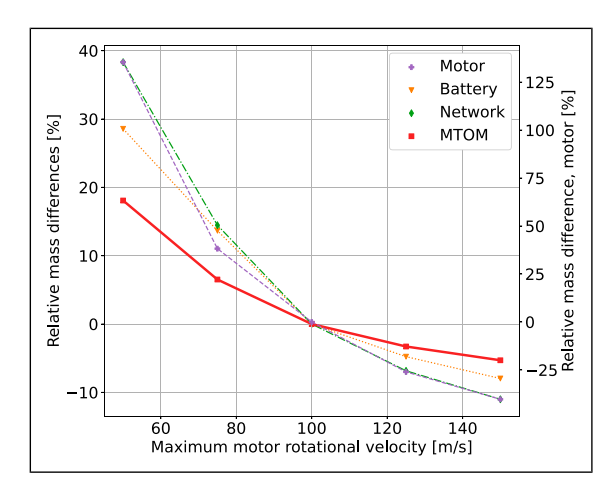


Figure 10. Effects of motor efficiency variations.

iterator creates a corresponding motor geometry with the highest nominal efficiency for the desired performance given geometric limits. The plot shows the motor sized for this aircraft has a nominal efficiency of 94%. However, over the full mission, the average efficiency shows closer to 85%. This is due to the chosen hybridization strategy. If the motor was used in a binary fashion, either used at maximum boost power or switched off, then it would actually operate at its nominal efficiency. As the motor is used at a lower power setting for all of the segments, this efficiency drops considerably. The lower the actual power setting, the higher the iron and copper losses in the machine, due to the electric fields and magnetism. The results show that the difference between nominal efficiency and real efficiency can be large for a full flight mission. For this BTF aircraft, the motor efficiency assumption can change the MTOM by more than 9% (+5% - -4%). Hence, a credible aircraft design should not be simulated based on nominal or maximal motor efficiency alone, but efforts should be made to find a realistic value for an average efficiency for the full flight profile.

Another interesting parameter to consider for the electric machine is the maximum rotational velocity of the rotor. Higher rotational velocities reduce the necessary torque to transmit the required power. With a lower torque, the required current in the motor can decrease and its efficiency increases. For a modern motor with current technology level, a tip rotational speed of 100 m/s is a sensible upper limit. Figure 11 shows that variations from this value can have a visible impact on the network performance and MTOM of the aircraft. Over the full range it shows how the motor mass changes from +140% to -28% of the baseline value. While velocities far in excess of 100 m/s will require more consideration in the design of the motor due to high centrifugal forces, the graph shows the potential benefits obtainable by further research and development in this area. The curves also show an asymptotic nature, indicating diminishing returns for much higher speeds. Eventually, additional structural



**Figure 11.** Effects of variations in the maximum allowed motor rotational velocity.

and material requirements will increase the motor mass again, although they are not modeled explicitly in this simulation. For more realistic values of current performance below the reference value, it can be seen that the graphs are increasing exponentially for lower rotational speeds. Halving this value will increase the network mass by about 40% and even the MTOM by about 18%, showing the critical impact of this parameter on motor performance and efficiency.

The results from both Figures 10 and 11 show the importance of utilizing proper motor performance models in electric aircraft design. Constant efficiency assumptions only hold when the motor is used close to its design power, and small internal changes can have a large influence on the total motor performance and efficiency.

# Fully electric regional aircraft

The second case study considers a FE regional aircraft. The aircraft is designed with 19 seats and is propelled by two electric motors. The required mission energy is stored in battery packs in the wing as shown in Figure 12. Table 6 shows key performance parameters characterizing the baseline aircraft.

Table 7 shows the selected input parameter choices taken to simulate the electrical components of the propulsion architecture for this baseline case. In order to have a better comparability, the network inputs are kept the same as for the BTF baseline case. The HVDC cable length has been reduced to 5 m, due to the smaller size of the FE aircraft. The resulting aircraft is presented in a mass breakdown in Table 8, including a detailed breakdown of the individual network components and their contribution to the total masses.

Power converters. The resulting curves for changes in semiconductor materials and switching frequencies presented in Figures 13 and 14 show a similar behavior to the BTF case. As the switching frequency increases, the mass of the power converters decreases. However, also the

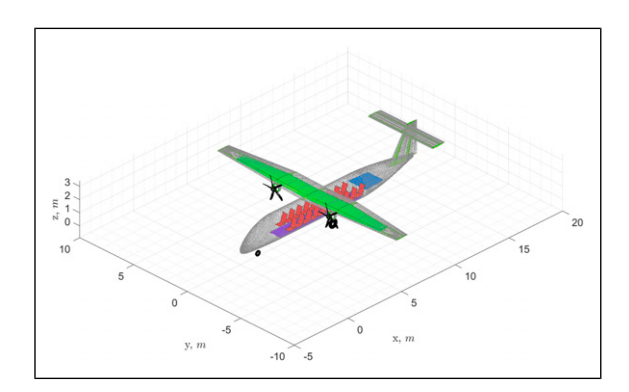


**Figure 12.** 19-passenger FE commuter aircraft baseline design.

**Table 6.** Key design parameters of the 19-passenger FE commuter aircraft.

Parameter	Value
Wing loading	2712 N/m <sup>2</sup>
Power loading	0.0948 N/W
Number of passengers	19
Cruise speed	113.75 m/s
Cruise altitude	3658 m
Wing aspect ratio	9
Wing taper ratio	0.45
Wing sweep	0°

**Table 7.** Electric network sizing input data of the FE commuter aircraft.

Value
30 kHz
Si
2LC
2000 V
Cu
5 m
1.51 MW
3.41 GJ
2
PPSM
500 Wh/kg

conversion efficiency decreases and thus more energy is required leading to larger batteries. As for this FE case the network is a larger fraction of the total aircraft mass, mass changes are more pronounced with a larger impact on the MTOM. The relative changes of the converters over the full range of investigated frequencies is very similar to the BTF case, ranging from +55% to -45% of the baseline value in both cases. Thus, the relative changes as a function of frequency or material do not depend on the

**Table 8.** Mass breakdown of the FE commuter aircraft baseline.

	Mass [kg]	% MTOM	% Network
МТОМ	8612	100.0	_
OEM	6807	79.0	_
Network	3518	40.8	100.0
Battery	2710	31.5	77.0
Motor	457	5.31	13.0
HVDC	69.8	0.81	1.98
DC/DC	65.I	0.76	1.85
DC/AC	125	1.45	3.55

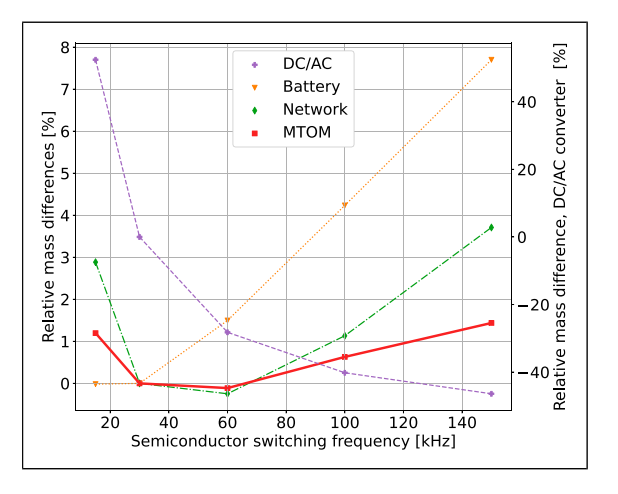


**Figure 13.** Effects of switching frequency variations using Sibased power electronics.

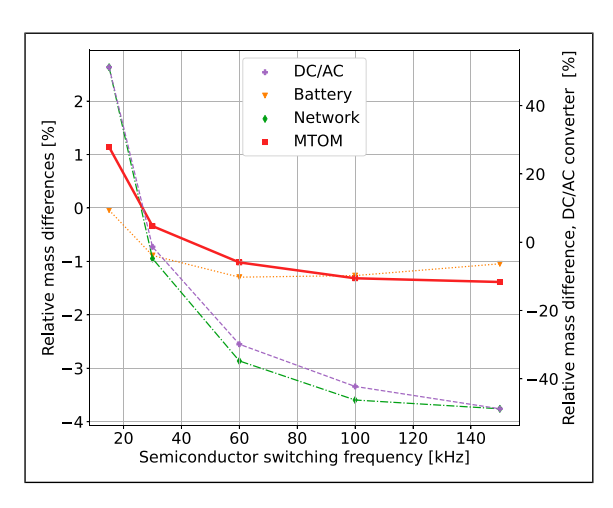


**Figure 14.** Effects of switching frequency variations using SiC-based power electronics.

network size or architecture. The reduction in efficiency over the investigated range has a similar effect on the FE aircraft, resulting in a 7.5% increase in battery mass versus 8% in the BTF case for Si-based converters. The optimum frequency range between 30 and 60 kHz is visible again, with a small bias towards 60 kHz as a more optimal value.

The SiC results in Figure 14 show differences to the BTF curves (Figure 6). While for both designs the

reductions in converter mass and the increase in battery mass are opposite yet approximately equal, for the FE case the influence on the total battery mass and thus on the MTOM is much smaller. Due to the higher network mass fraction of the battery in the FE case, the initial network weight reductions are smaller compared to the BTF, and thus the overall impact of the power electronics on the total mass is smaller for this aircraft. The differences are also influenced by the higher total installed power in the BTF (3.6x) and associated differences in the resulting performance of the converter components as they are operating at different design points.

Power distribution. The power distribution plots in Figures 15 and 16 again show an overall similar behavior to the BTF, with differences in the relative impact of the components. For both cable materials, the changes in voltage lead to slightly smaller relative changes in the cable mass. As the cables are shorter compared to the BTF case, installation effects have a relatively larger impact. Similar to the power electronics, the effect on the battery and total mass is reduced due to the smaller overall system as power requirements are lower. Using Cu wires, changes

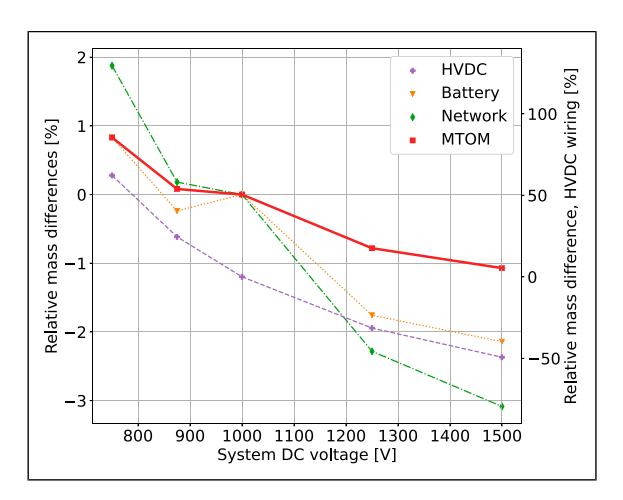


Figure 15. Effects of DC voltage variations using Cu wiring.

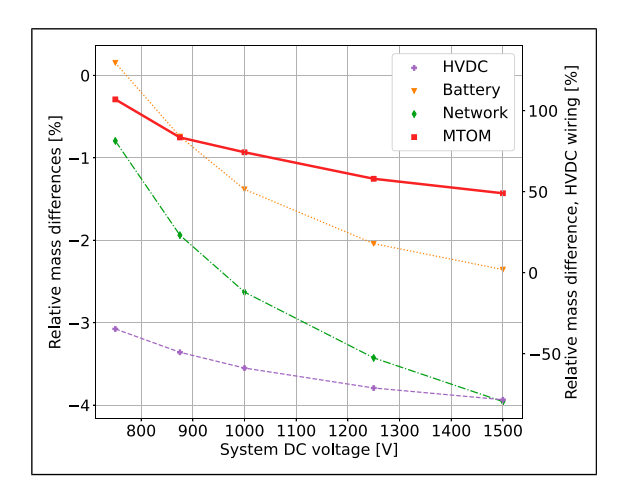


Figure 16. Effects of DC voltage variations using Al wiring.

of +65% to -55% can be observed. As the total size of the network is much smaller, these only have a small impact on the MTOM, in the range of +1% to -1%. For the Al cables, this effect is similar. While using Al shows a large reduction compared to Cu at all voltage levels, this difference becomes smaller for higher voltages (from 95% decreasing to 25% of the baseline value). Hence also the overall range of MTOM changes is smaller. For low voltages, the benefits of Al result in a 1.5% reduction compared to Cu wiring. For high voltages, this benefit reduces to about 0.5% MTOM reduction.

Thus, for smaller aircraft with short cables, the effects of changes in the HVDC wiring are small. The benefits of using Al cables over conventional and cheaper Cu cables are small. This holds especially for higher voltages, when the current to be transmitted is lower.

Changes in the cable length shown in Figure 17 have a higher impact on the FE aircraft. The plot shows a linear change of the masses. Halving the length corresponds to a 50% reduction, doubling the length to a 110% increase. The slightly larger-than-proportional increase in mass for increasing length results from a corresponding increase in total required power and energy for the increasing aircraft size. Doubling the cable length also leads to a 0.5% increase in the battery mass, and thus a total 1% higher MTOM (1 passenger) for this network.

Electric motor. While the effects of power electronics and wiring on this aircraft design are smaller due to the lower maximum power requirements and size, the electric motors still have a visible effect on the total aircraft.

The effects of constant motor efficiency assumptions on the FE aircraft are shown in Figure 18. Regarding the motor mass, it can be seen that for increasing efficiency the mass is decreasing exponentially, albeit the changes are small and in a range of +7.5% to -4.5%. The efficiency changes have a much larger impact on the

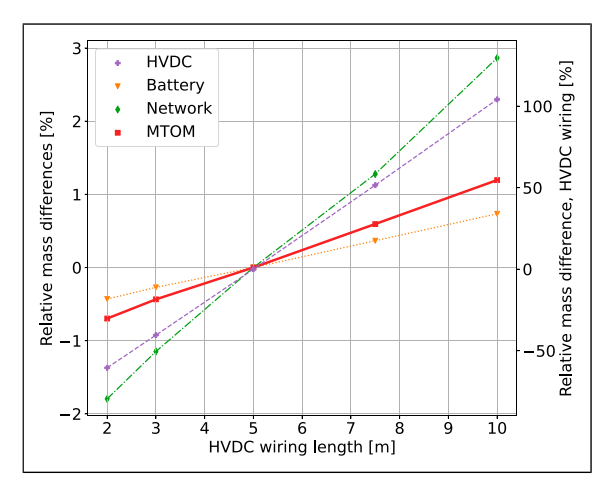


**Figure 17.** Effects of HVDC cable length variations using Cu wiring.

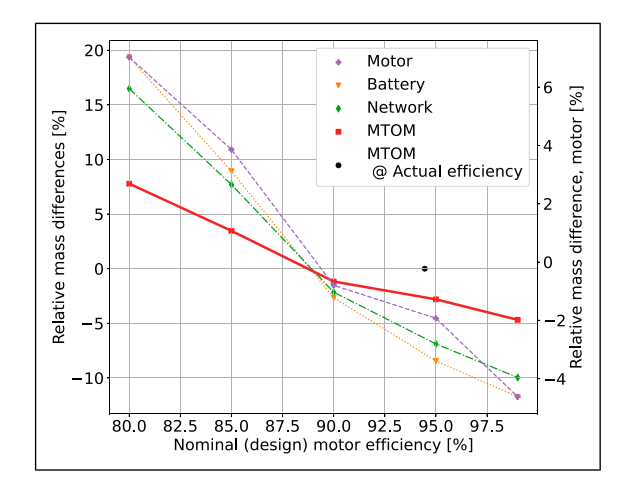


Figure 18. Effects of motor efficiency variations.

battery masses, changing in the range of +20% to -12%. With both battery and motor changes summed together, the total aircraft mass changes by 12% over the investigated range.

Similar to the observations for the BTF, the results for the design without a fixed efficiency show a higher MTOM compared to the relevant one at a given efficiency. When the motor is allowed to be internally optimized for the given conditions in length and diameter, a peak efficiency of about 94.5% is achievable. Comparing the optimized result with the fixed results show an equivalent average efficiency of 88%. This value is slightly higher than for the BTF case. In this aircraft, the motor is the primary means of power, and hence the motor is running closer to its design power for the majority of the mission. Thus its average value is closer to peak design efficiency. However, a reduction of about 5% still applies over the full mission. Hence, even for high continuous power applications a reduced overall motor efficiency should be assumed when sizing the powertrain in conceptual design using simple models that do not account for performance changes in different flight phases.

Figure 19 shows the effects for a change in maximum rotational velocity. Comparing the results to the BTF in Figure 11, it shows that the relative mass changes for the motor itself are similar, although the FE results are a bit higher. For the maximum velocity of 150 m/s in the BTF case, the relative reduction is about 40% vs. 50% in the electric case.

While these results show that the relative effects of changes in the rotational velocity for the motor are nearly constant for the same motor type, the total effects of the changing motor masses and efficiencies are not. For the FE case the changes in battery mass are much smaller, varying only in the order of +21% to -3%, instead of +28% to -8% for the BTF. The combination of these two mass changes leads to MTOM variations of +16% to -3%. These results show that for the smaller aircraft, the battery is dominating the network design space. For motors with a high efficiency, increasing the

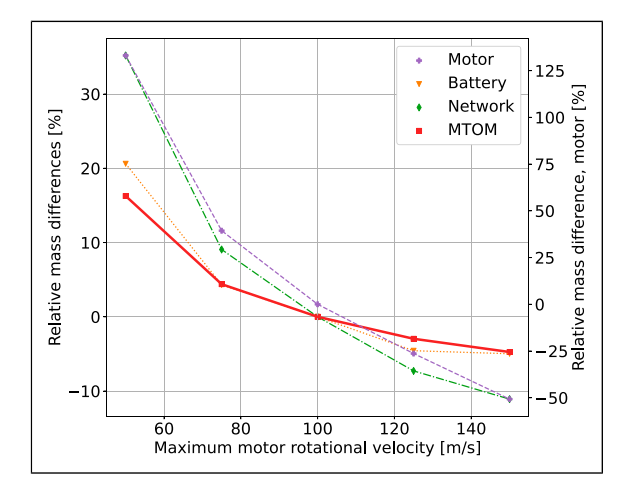


**Figure 19.** Effects of variations in the maximum allowed motor rotational velocity.

rotational velocity beyond 100 m/s results in a smaller motor and better efficiency, but the further mass reductions are barely reflected in the final MTOM. On the other hand, for lower performing motors, the additional mass and lower efficiency increases the total aircraft mass and power requirements, and thus necessitates a larger battery, further increasing the MTOM.

Thus, it shows that for smaller aircraft with lower maximum power requirements, the most influential parameters are the battery and the motor performance, while the power electronics and distribution are only of secondary nature.

# Summary

Following the sensitivity studies into the selected network parameters for both the BTF and FE results, the most relevant results are summarized in Table 9. The table highlights the changes in MTOM for both aircraft concepts due to variations in the components for ranges supported by the relevant scientific literature. Furthermore, comments on the largest challenges for the implementation of each individual component are added, together with relevant literature to support the chosen ranges and for further information. This should not mean that the parameters and ranges in Table 9 are conclusive - but that these ranges as considered feasible for electric aircraft networks in the near future. Performance can always be improved by novel developments and technologies.

#### Limitations

A selection of important parameters is investigated. This selection is based on current network literature. However, a real energy network contains additional design features which will influence the final aircraft and network design performance.

The presented designs size the necessary network for a feasible aircraft, but do not consider any redundancies. This is in line with current conceptual design literature. In

Table 9. Summary of sensitivity study results for BTF and FE aircraft for the ranges of values supported by literature; including relevant challenges per network parameter.

Parameter	Nominal value	Investigated range	Impact on BTF MTOM	Impact on FE MTOM	Challenges	References
Semiconductor	Σ	Si/SiC		I	WBG wafer cost     Certif device availability	22,23,24, 27,20,11,
Semiconductor switching frequency (Si)	30 kHz	15 kHz - 150 kHz	(+1.5%) – (0%)	(+1.5%) - (-0.1%)	• Devices specific sweet spot $(f_s \text{ vs. } \eta)$	26,25
Semiconductor switching frequency	30 kHz	15 kHz - 150 kHz	(+1.5%) – (–4.5%)	(+1%) - (-1.5%)		
(SiC) Cable material	ਹੋ	Cu/Al	1		<ul> <li>Arcing &amp; insulation</li> </ul>	22,28,21
DC voltage (Cu)	2000 V	1500 V - 3000 V	(+3%) - (-7%)	(%1-) - (%1+)	<ul> <li>Regulations prohibiting</li> </ul>	16,34,29,
DC voltage (AI)	2000 V	1500 V - 3000 V	(-5%) - (-9%)	(-0.5%) - (-1%)	Al near motor (FAA)	24,23
Cable length	10 m / 5 m	l m - 20 m	(-4%) - (+8%); for range 5-20 m	(-1%) - $(+1%)$ ; for range 2-10 m	<ul> <li>Material cost</li> <li>Battery placement</li> </ul>	
Motor efficiency	%56	%66 - %06	(+5%) - (-4%)	(+8%) - (-5%)	<ul> <li>Specific architecture</li> </ul>	11,19,15,
Motor rotational	100 m/s	50 m/s - 150 m/s	(%/-) - (%61+)	(+16%) - (-5%)	<ul> <li>Off-design performance</li> </ul>	23,21,20 30
sbeed						

a certifiable aircraft design, mass penalties due to redundant systems have to be included, leading to larger sensitivities of all network design parameters on a final aircraft concept.

## **Conclusions**

This paper presents sensitivity studies for a range of influential parameters on the energy network for (hybrid-) electric aircraft on a physical parameter level. For this, a detailed energy network model that does not rely on statistical values for estimation of performance and mass, but has individual models for each major network component is used in combination with conceptual aircraft design software. Parameters defining the power conversion, power distribution and electric motor are investigated in sweeps for two case studies: A 50-passenger Boosted-Turbofan (BTF) regional jet and a 19-passenger Fully-Electric (FE) commuter aircraft.

Results showed that for power electronics Silicon Carbide (SiC)-based semiconductors at high switching frequencies (>60 kHz) provide the best overall mass and efficiency results. Si-based semiconductors have an optimal range between 30 and 60 kHz, with increases in overall mass outside this range. On the low side this is due to higher component mass, on the high side due to decreased component efficiency.

For power distribution, a clear correlation was found between higher Direct Current (DC) and a significant reduction in the overall aircraft mass, since higher voltages reduce the required current in the cable and thus increase the transmission efficiency. This is however limited by the corresponding increase in the risk of arcing, which needs to be considered in the design. Further improvement can be obtained by using aluminum wires instead of copper: while aluminum has a lower current density and thus needs larger cables by volume, its much lower density can still lead to reductions up to 70% of the High-Voltage Direct Current (HVDC) cable mass for a given voltage.

Irrespective of voltage or material, cable length is a clear driver of the overall weight. The closer the batteries are to the motors, the less cable length will be needed. For the BTF, a doubling in the cable length (e.g. moving the batteries from wing to fuselage) can increase the Maximum Take-Off Mass (MTOM) by up to 8%.

Electric motors are often simply characterized by their design efficiency for use in conceptual design. In reality the efficiency of the motor depends on the actual power setting, and is thus variable throughout the mission. For a full flight profile, the effective mission-average efficiency can be significantly lower than the maximum motor efficiency, and this performance penalty should be taken into account for a credible electric aircraft design concept. Changes in motor performance parameters such as the maximum rotational velocity of the rotor tips, and its implications on the maximum torque also have a significant impact on the size and efficiency of the final motor, and thus on the

total aircraft design. Comparing the results from the BTF and the FE case, it shows that the effects of variations in the network parameters are more pronounced in the BTF. Although the electric network is only a small part of the full propulsion system, the power and energy requirements are significantly higher compared to the electric commuter aircraft, and thus the individual components are larger. The results show that the specific choices are more relevant for networks with higher power requirements and can result in changes of over 10% of the MTOM within the investigated ranges. For the FE case the sensitivities on the MTOM are much smaller and the resulting battery mass is the more limiting factor. Changes in component efficiency outrank changes in component mass as their net effect on the battery size is larger.

Thus, for large aircraft the network is mostly sensitive to changes in the required power. For small aircraft it is mostly sensitive to changes in the required mission energy.

Future research could focus on investigating the effects on other network architectures, such as a serial electric power train, where batteries are a less important aspect of the total network.

#### Author's note

The research presented in this publication was performed under the European Union's Horizon 2020 Clean Sky 2 project Credible HYbrid-eLectric Aircraft (CHYLA).

### **Acknowledgements**

The authors wish to thank Jan Göing, Patrick Mayer and Jens Friedrichs from the Institute of Jet Propulsion at TU Braunschweig for providing the propulsion models in the energy network; and Lukas Radomsky, Lucas-Vincent Hanisch, Regine Mallwitz and Markus Henke from the Institute for Electrical Machines, Traction and Drives at TU Braunschweig for providing the electric network and machine codes for the network models. Furthermore, the authors would like to thank Vincent Bonnin and Maurice Hoogreef from the Department of Aerodynamics, Wind Energy, Flight Performance and Propulsion of the Aerospace Engineering Faculty of Delft University of Technology for the provided baseline aircraft designs used in this publication.

## **Declaration of conflicting interests**

The author(s) declared no potential conflicts of interest with respect to the research, authorship, and/or publication of this article.

# **Funding**

The author(s) disclosed receipt of the following financial support for the research, authorship, and/or publication of this article: This project has received funding from the Clean Sky 2 Joint Undertaking (JU) under grant agreement No 101007715. The JU receives support from the European Union's Horizon 2020 research and innovation program and the Clean Sky 2 JU members other than the Union.

#### **ORCID iD**

Nicolas FM Wahler https://orcid.org/0000-0001-6245-6052

#### Notes

- 1. https://suave.stanford.edu/.
- 2. https://www.mh-aerotools.de/airfoils/javaprop.htm.
- 3. https://www.gasturb.com/.

#### References

- 1. Leipold A, Aptsiauri G, Ayazkhani A, et al. Depa 2050–development pathways for aviation up to 2050. *Technical report, German Aerospace Centre (DLR)* 2021.
- Hoogreef MF and Bonnin VO. Scalability analysis of radical technologies to various aircraft class-part I: initial designs.
   In: 33rd Congress of the International Council of the Aeronautical Sciences. 4-9 September 2022, Stockholm, Sweden, p.248.
- Bonnin VO and Hoogreef MF. Scalability analysis of radical technologies to various aircraft class-part II: sensitivity analysis. In: 33rd Congress of the International Council of the Aeronautical Sciences. 4-9 September 2022, Stockholm, Sweden, p.481.
- de Vries R, Brown MT and Vos R. A preliminary sizing method for hybrid-electric aircraft including aero-propulsive interaction effects. In: 2018 Aviation Technology, Integration, and Operations Conference, 25-29 June 2018, Atlanta, GA, USA, p. 4228.
- Bowman CL, Felder JL and Marien TV. Turbo-and hybridelectrified aircraft propulsion concepts for commercial transport. In: 2018 AIAA/IEEE Electric Aircraft Technologies Symposium (EATS). 12-14 July 2018, Cincinnati, OH, USA, p. 4984.
- Sahoo S, Zhao X and Kyprianidis K. A review of concepts, benefits, and challenges for future electrical propulsionbased aircraft. *Aerospace* 2020; 7(4): 44.
- Botero EM, Wendorff A, MacDonald T, et al. Suave: an open-source environment for conceptual vehicle design and optimization. In: 54th AIAA aerospace sciences meeting, 4-8 January 2016, San Diego, California, USA, p. 1275.
- Falck RD, Chin J, Schnulo SL, et al. Trajectory optimization of electric aircraft subject to subsystem thermal constraints.
   In: 18th AIAA/ISSMO multidisciplinary analysis and optimization conference, 5-9 June 2017, Denver, Colorado, USA, p. 4002.
- 9. Freeman J, Osterkamp P, Green M, et al. Challenges and opportunities for electric aircraft thermal management. *Aircraft Eng Aero Technol: Int J* 2014.
- Schiltgen BT and Freeman J. Aeropropulsive interaction and thermal system integration within the eco-150: a turboelectric distributed propulsion airliner with conventional electric machines. In: 16th AIAA aviation technology, integration, and operations conference, 13-17 June 2016, Washington, DC, USA, p. 4064.
- 11. Vratny PC, Forsbach P, Seitz A, et al. Investigation of universally electric propulsion systems for transport aircraft. 29th congress of the international council of the aeronautical sciences, 7-12 September 2014. St. Petersburg, Russia, p. 744.
- 12. Pornet C and Isikveren AT. Conceptual design of hybridelectric transport aircraft. *Prog Aero Sci* 2015; 79: 114–135.
- 13. Gesell H, Wolters F and Plohr M. System analysis of turboelectric and hybrid-electric propulsion systems on a regional aircraft. *Aeronaut J* 2019; 123(1268): 1602–1617.
- Jansen R, Bowman C and Jankovsky A. Sizing power components of an electrically driven tail cone thruster and a range extender. In: 16th AIAA aviation technology,

- integration, and operations conference, 13-17 June 2016, Washington, DC, USA, p. 3766.
- Köhler J and Jeschke P. Conceptual design and comparison of hybrid electric propulsion systems for small aircraft. CEAS Aeronaut J. 2021; 12(4): 907–922.
- Vratny PC, Kuhn H and Hornung M. Influences of voltage variations on electric power architectures for hybrid electric aircraft. CEAS Aeronaut J 2017; 8: 31–43.
- Stückl S, van Toor J and Lobentanzer H. VOLTAIR-the allelectric propulsion concept platform—a vision for atmospheric friendly flight. In: Proceedings of the 28 th International Congress of The Aeronautical Sciences. 23-28 September 2012, Brisbane, Australia, p.521.
- 18. Isikveren AT, Seitz A, Vratny PC, et al. Conceptual studies of universally-electric systems architectures suitable for transport aircraft. In: 61. Deutscher Luft und Raumfahrt Kongress 2012, 10-12 September 2012, Berlin, Germany.
- Ibrahim K, Sampath S and Nalianda D. Optimal voltage and current selection for turboelectric aircraft propulsion networks. *IEEE Trans Transp Electrific* 2020; 6(4): 1625–1637.
- Barzkar A and Ghassemi M. Components of electrical power systems in more and all-electric aircraft: a review. *IEEE Trans Transp Electrific* 2022; 8(4): 4037–4053.
- Brelje BJ and Martins JR. Electric, hybrid, and turboelectric fixed-wing aircraft: a review of concepts, models, and design approaches. *Prog Aero Sci* 2019; 104: 1–19.
- Schefer H, Fauth L, Kopp TH, et al. Discussion on electric power supply systems for all electric aircraft. *IEEE Access* 2020; 8: 84188–84216.
- Barzkar A and Ghassemi M. Electric power systems in more and all electric aircraft: a review. *IEEE Access* 2020; 8: 169314–169332.
- Dorn-Gomba L, Ramoul J, Reimers J, et al. Power electronic converters in electric aircraft: current status, challenges, and emerging technologies. *IEEE Trans Transp Electrific* 2020; 6(4): 1648–1664.
- Han D, Ogale A, Li S, et al. Efficiency characterization and thermal study of gan based 1 kw inverter. In: 2014 IEEE Applied Power Electronics Conference and Exposition-APEC 2014. 16-20 March 2024, Fort Worth, TX, USA, pp. 2344-2350.
- 26. Nawawi A, Tong CF, Yin S, et al. Design and demonstration of high power density inverter for aircraft applications. *IEEE Trans Ind Appl* 2016; 53(2): 1168–1176.
- Wileman A, Aslam S and Perinpanayagam S. A road map for reliable power electronics for more electric aircraft. *Prog Aero Sci* 2021; 127: 100739.
- Vazquez T, Teulet P, Valensi F, et al. Arc fault power balance in ac and dc electrical aeronautic networks: influence of pressure and cable material. J Phys D Appl Phys 2020; 54(8): 085207.
- Malburg L, Moonen N and Leferink F. The changing electromagnetic environment onboard all-electric aircraft, an emc perspective. In: 2021 IEEE International Joint EMC/SI/ PI and EMC Europe Symposium. 26 July-13 August 2021, Raleigh, NC, USA, pp. 845-850.
- Wahler N, Radomsky L, Hanisch L, et al. An integrated framework for energy network modeling in hybrid-electric aircraft conceptual design. In: AIAA AVIATION 2022 forum, 27 June-1. Chicago, IL: & Virtual, July, 2022, p. 3741.
- 31. Wahler N, Maruyama D and Elham A. Credibility-based multidisciplinary design optimisation of hybrid and fully electric aircraft. *J Aircraft* 2025, Epub ahead of print 28 Januar 2025.

- 32. Brown G. Weights and efficiencies of electric components of a turboelectric aircraft propulsion system. In: 49th AIAA aerospace sciences meeting including the new horizons forum and aerospace exposition, 4-7 January 2011, Orlando, Florida, USA, p. 225.
- 33. Aigner B, Nollmann M and Stumpf E. Design of a hybrid electric propulsion system within a preliminary aircraft design software environment. 67 Deutsche Gesellschaft für Luft- und Raumfahrt-Lilienthal-Oberth eV Germany, 4-6 September 2018. Friedrichshafen, Germany.
- 34. Lowe A and Mavris DN. Technology selection for optimal power distribution efficiency in a turboelectric propulsion system. *SAE Int J Aerosp* 2012; 5: 425–437.
- Cozzolino A, Apuleo G and Dalesio P. Technology readiness assessment and performance forecast on a 19 seats E-STOL EIS 2032. J Phys: Conf. Ser 2023; 2526: 012016.
- Wahler N, Maruyama D and Elham A. Credibility-based multidisciplinary design optimisation of electric aircraft. In: AIAA SCITECH 2023 forum, 23-27 January 2023, National Harbor, MD, USA & Online, p. 1847.
- 37. Lüeck S, Göeing J, Wittmann T, et al. Propeller design and performance evaluation with partially prescribed velocity distribution. In: Proceedings of global power and propulsion society, 18-20 October 2021, Xi'an, China, p.328.
- Adkins CN and Liebeck RH. Design of optimum propellers. J Propul Power 1994; 10(5): 676–682.
- Branlard E. Wind turbine aerodynamics and vorticity-based methods: fundamentals and recent applications. Springer; 2017.
- 40. Goeing J, Bode C, Friedrichs J, et al. Performance simulation of roughness induced module variations of a jet propulsion by using pseudo bond graph theory. In: ASME Turbo Expo: Power for Land, Sea, and Air, 21-25 September 2020, Online.
- Kashihara Y and Itoh J. The performance of the multilevel converter topologies for pv inverter. In: 2012 7th International Conference on Integrated Power Electronics Systems (CIPS). 6-8 March 2012, Nuremberg, Germany.
- 42. Bentheimer C, Islami A, Mainusch S, et al. Highly efficient SiC inverter for aircraft application with innovative thermal management. In: PCIM Europe 2019; International Exhibition and Conference for Power Electronics, Intelligent Motion. *Renewable Energy and Energy Management.* 7-9 May. 2019; 1190–1197.
- 43. Fritz N, Rashed M and Klumpner C. Power density optimization of a dc/dc converter for an aircraft supercapacitors energy storage. In: 2018 IEEE International Conference on Electrical Systems for Aircraft, Railway, Ship Propulsion and Road Vehicles & International Transportation Electrification Conference (ESARS-ITEC). 7-9 November 2018, Nottingham, UK.
- 44. Yapa R, Forsyth AJ and Todd R. Analysis of sic technology in two-level and three-level converters for aerospace applications. In: 7th IET International Conference on Power Electronics, Machines and Drives (PEMD 2014), 8-10 April 2014, Manchester, UK.
- Laird I, Yuan X, Scoltock J, et al. A design optimization tool for maximizing the power density of 3-phase dc-ac

- converters using silicon carbide (sic) devices. *IEEE Trans Power Electron* 2017; 33(4): 2913–2932.
- 46. Schobre T and Mallwitz R. Automated design method for sine wave filters in motor drive applications with SiC-inverters. In: 2020 22nd European conference on power electronics and applications (EPE'20 ECCE Europe), 7-11 September 2020, Lyon, France.
- Shirabe K, Swamy M, Kang JK, et al. Advantages of high frequency PWM in AC motor drive applications. In: 2012 IEEE Energy Conversion Congress and Exposition (ECCE), 15-20 September 2012, Raleigh, NC, USA, pp. 2977–2984.
- 48. Schobre T, Langmaack N and Mallwitz R. Analytical modeling of ripple currents in a drive inverter with a LC sine wave filter. PCIM Europe digital days 2020; International Exhibition and Conference for Power Electronics, Intelligent Motion, *Renewable Energy and Energy* Management, 7-8 July 2020, Online, pp. 402-406.
- Langfermann S. Optimierung einer Sinusfilterdrossel für eine SiC-Anwendung. Induktiviäten in der Leistungselektronik, In: Cluster Leistungselektronik. 20-21 July 2022. Nuremberg, Germany.
- Ejury J. Design Note DN2013-01 Buck converter design. Durham, NC, USA: Infineon Technologies North America, 2013.
- DIN. DIN 57100-430:1981-06: Errichten von Starkstromanlagen mit Nennspannungen bis 1000 V Schutz von Leitungen und Kabeln gegen zu hohe Erwärmung. 1981.
- 52. Tariq M, Maswood AI, Gajanayake CJ, et al. Aircraft batteries: current trend towards more electric aircraft. *IET Electr Syst Transp* 2017; 7(2): 93–103.
- 53. Felder J, Tong M and Chu J. Sensitivity of mission energy consumption to turboelectric distributed propulsion design assumptions on the N3-X hybrid wing body aircraft. In: 48th AIAA/ASME/SAE/ASEE joint propulsion conference & exhibit, 30 July-1 August 2012, Atlanta, Georgia, USA, p. 3701
- 54. Henke PM and Tareilus G. SiC boost converter with high power density for a battery electric sports car. In: 11th symposium on hybrid and electric vehicles, February 18th and 19th, 2014, Braunschweig, Germany.
- Hofmann M. Air-cooled 40 kW SiC-inverter. Fraunhofer Institute for Integrated Systems and Device Technology.
- Elmendorp R, Vos R and La Rocca G. A conceptual design and analysis method for conventional and unconventional airplanes. In: 29th Congress of the International Council of the Aeronautical Sciences, 7-12 September 2014, St. Petersburg, Russia, p.776.
- 57. Hoogreef MF, Bonnin VO, Santos BF, et al. Scalability assessment of hybrid-electric technology application to various aircraft classes-an overview of opportunities and challenges. In: Aerospace Europe Conference 2023–10th EUCASS–9th CEAS. 9-13 July 2023, Lausanne, Switzerland.
- 58. Wahler N, Radomsky L, Hanisch L, et al. A credibility-based criterion for the assessment of futuristic aircraft concepts. In: 33rd Congress of the international council of the aeronautical sciences, 4-9 September 2022, Stockholm, Sweden, p. 850.